

1 Climatic Controls on Metabolic Constraints in the Ocean

2 Precious Mongwe¹, Matthew Long², Takamitsu Ito³, Curtis Deutsch⁴, and Yeray
3 Santana-Falcón⁵

4 ¹Southern Ocean Carbon Climate Observatory (SOCCO), CSIR, Cape Town, South Africa

5 ²Oceanography Section, Climate and Global Dynamics Laboratory, National Center for Atmospheric Research,
6 Boulder, CO, United States of America

7 ³School of Earth and Atmospheric Sciences, Georgia Institute of Technology, Atlanta, Georgia United States of
8 America

9 ⁴Department of Geosciences, Princeton University, Princeton, NJ, United States of America

10 ⁵CNRM, Université de Toulouse, Météo-France, CNRS, Toulouse, 31057, France

11 **Corresponding Author:** Precious Mongwe (pmongwe@csir.co.za)

13 Abstract

14 Observations and models indicate that climate warming is associated with the loss of dissolved
15 oxygen from the ocean. Dissolved oxygen is a fundamental requirement for heterotrophic marine
16 organisms (except marine mammals) and, since the basal metabolism of ectotherms increases
17 with temperature, warming increases organisms' oxygen demand. Therefore, warming and
18 deoxygenation pose a compound threat to marine ecosystems. In this study, we leverage an
19 ecophysiological framework and compilation of empirical trait data quantifying the temperature
20 sensitivity and oxygen requirements of metabolic rates for a range of marine species
21 ("ecotypes"). Using the Community Earth System Model Large Ensemble, we investigate how
22 natural climate variability and anthropogenic forcing impact the ability of marine environments
23 to support aerobic metabolisms on interannual to multi-decadal timescales. Warming and
24 deoxygenation projected over the next several decades will yield a reduction in the volume of
25 viable ocean habitat. We find that fluctuations in temperature and oxygen associated with natural
26 variability are distinct from those associated with anthropogenic forcing in the upper ocean.

27 Further, the joint temperature-oxygen anthropogenic signal emerges sooner than independently
28 from natural variability. Our results demonstrate that anthropogenic perturbations underway in
29 the ocean will strongly exceed those associated with the natural system; in many regions,
30 organisms will be pushed closer to or beyond their physiological limits, leaving the ecosystem
31 more vulnerable to extreme temperature-oxygen events.

Deleted: ¶

Formatted: Border: Top: (No border), Bottom: (No border),
Left: (No border), Right: (No border), Between : (No border)

Deleted: s

34 **1. Introduction**

35 Dissolved oxygen (O₂) is a fundamental metabolic requirement for heterotrophic marine
36 organisms, excluding marine mammals (Portner, 2002; Keeling et al., 2010; Tiano et al., 2014).
37 O₂ is declining due to warming, a tendency long predicted by models (Keeling et al., 2010; Long
38 et al., 2016; Oschlies et al., 2018) and recently found evident at the global scale in compilations
39 of in situ observations (Schmidtko et al., 2017; Ito et al., 2017). Deoxygenation is driven by the
40 direct effect of reduced oxygen solubility with warming compounded by buoyancy-induced
41 stratification in the upper ocean, which weakens the ventilation-mediated supply of fresh oxygen
42 to the ocean interior. While the full ecological impacts of ocean deoxygenation remain uncertain,
43 it is clear that the physiological impacts of oxygen loss on marine organisms can be considered
44 explicitly in the context of warming: basal metabolic rates for ectothermic organisms depend on
45 ambient temperature and increase with warming (Gillooly et al., 2001); thus, higher temperatures
46 impose additional demand for oxygen to sustain aerobic respiration (Deutsch et al., 2015).
47 Consequently, as the ocean warms, even present-day oxygen distributions may be insufficient to
48 meet the oxygen demands of organisms living near key physiological thresholds (Deutsch et al.,
49 2022).

50
51 While model projections clearly demonstrate that warming and deoxygenation are consequences
52 of human-driven climate change, it is important to recognize that natural climate variability also
53 produces important fluctuations in these quantities. Indeed, evidence suggests that natural
54 variability contributes to hypoxic events, such as those observed in the California Current, where
55 fish and benthic-organism mortality has been associated with low-O₂ waters impinging on the
56 continental shelf (Poza Buil and Di Lorenzo, 2017; Howard et al., 2020). A clear understanding
57 of how natural climate variability drives fluctuations in metabolic state and the associated
58 implications for organisms is a critical context in which to view long-term climate warming.
59 Given that the natural system is highly dynamic, climate change signals are often masked by
60 decadal-scale variability (Ito and Deutsch, 2010). While numerous authors have considered
61 detection and attribution of climate change for physical and biogeochemical variables (Rodgers
62 et al., 2015; Long et al., 2016; Schlunegger et al., 2019), comparatively little attention has been
63 devoted to explicitly characterizing the relative influence of natural and anthropogenic drivers of
64 changes in the ocean's capacity to support aerobic life. In this study, we approach this challenge

65 by leveraging the concept of the Metabolic Index (Φ) introduced by Deutsch et al. (2015). Φ is
66 based on the notion that aerobic organisms can persist only where the ambient oxygen partial
67 pressure (pO_2) is sufficient to meet the requirements of sustaining respiration. Φ incorporates an
68 explicit representation of the dependence of metabolic oxygen demand on temperature, thus
69 providing a framework to consider how joint oxygen and temperature variability constrain viable
70 habitat in the ocean.

71

72 Many ocean organisms may already be under threat from deoxygenation (Hoegh-Guldberg and
73 Bruno, 2010; Breitburg et al., 2018); however, ongoing climate-driven loss of oxygen raises
74 important questions about the future of marine ecosystems: How will anthropogenic changes in
75 dissolved oxygen and temperature impact the capacity of ocean habitats to support aerobic
76 metabolism? What is the spatial and temporal distribution of changes in the ocean's metabolic
77 state associated with climate variability? At what point can anthropogenic change in the ocean's
78 metabolic state be distinguished from natural variability? This study addresses these questions
79 using a combination of metabolic theory, a dataset set quantifying key physiological parameters
80 for a collection of marine species adapted to specific environments ("ecotypes"), and the oxygen
81 and temperature distributions simulated in the Community Earth System Model, version 1 Large
82 Ensemble (CESM1-LE), which includes 34 members simulating ocean biogeochemistry under
83 climate variability and change from 1920–2100 forced using historical data and the
84 Representative Concentration Pathway Scenario 8.5 (RCP85) (Kay et al., 2015; Long et al.,
85 2016).

86

87 This paper is organized as follows. Section 2 presents a brief overview of the relevant metabolic
88 theory, the associated empirical datasets, and describes our approach to analysis. In Section 3 we
89 present results quantifying the joint temperature-oxygen variability simulated in the CESM1-LE,
90 evaluating the spatiotemporal structure of variability in marine ecotype habitat, including long-
91 term trends based on the RCP8.5 scenario and time of emergence (ToE). The main outcomes of
92 the results are synthesized in Section 4 and summarized in Section 5.

93

94 **2. Datasets and methods**

95 **2.1 Metabolic index**

96 Empirical studies measuring thermal tolerance and oxygen requirements in the laboratory on an
97 array of marine organisms have enabled an assessment of lethal thresholds (Vaquer-Sunyer and
98 Duarte, 2008; Rosewarne et al., 2016). These data coupled with recent advances in a theoretical
99 framework enable both explanatory and predictive power in the context of a dynamic
100 environment (Deutsch et al., 2015; Penn et al., 2018; Howard et al., 2020). The fundamental
101 insights here are that basal metabolic rates for ectothermic marine organisms depend on ambient
102 temperature and generally increase with warming (Gillooly et al., 2001). Increasing basal
103 metabolic rates impose additional demand for oxygen. Organisms use oxygen dissolved in
104 seawater and acquisition tends to be limited by diffusive processes; thus, oxygen supply is
105 related to the ambient pO_2 . The ratio of oxygen supply to temperature-dependent demand
106 provides a critical indicator of the capacity for an organism to meet its metabolic requirements.
107 Deutsch et al. (2015) formalized these concepts into a quantity termed the “Metabolic Index
108 (Φ)”, which is defined as the ratio of oxygen supply to an organism’s resting metabolic demand.
109 Oxygen supply is parameterized according to a biomass-dependent scaling of pO_2 , capturing
110 variation in the efficiency with which organisms acquire and utilize O_2 . This can be expressed as

111 $S = \alpha_s B^\sigma pO_2$, where α_s represent gas transfer between an organism and its environment and B^δ
112 is the scaling of supply with biomass, B (Piiper et al., 1971). Gas supply is represented as an
113 Arrhenius function:

114
$$\alpha_s = \alpha_s \exp\left\{\frac{-E_s}{k_B} \left[\frac{1}{T} - \frac{1}{T_{ref}}\right]\right\}$$
 (1)

115
116 Resting metabolic demand is also expressed using the Arrhenius equation as

117
$$D = \alpha_D B^\delta \exp\left\{\frac{-E_d}{k_B} \left[\frac{1}{T} - \frac{1}{T_{ref}}\right]\right\}$$
 (2)

118 where α_D is a species-specific basal metabolic rate, E_d (eV) is the temperature dependence of
119 oxygen supply, T is temperature, T_{ref} is the reference temperature (15°C), and k_B is the
120 Boltzmann constant (Gillooly et al., 2001). Gas transfer is kinematically slow at low
121 temperatures, and hence organism viability can be limited by the energy to acquire oxygen at low
122 temperatures, thus E_o varies with temperature. Here we account for this by adding the
123 temperature dependence (dE_o/dT) to E_o in equations above ($E_o + \frac{dE_o}{dT}(T - T_{ref})$), using the mean

- Deleted: $\alpha_s B^\sigma pO_2$,
- Deleted:
- Deleted: α_s
- Deleted: is
- Deleted: a mass-normalized coefficient expressing the rate of

- Deleted:
- Deleted: can be
- Deleted: the
- Deleted: B^δ is the scaling of this rate with biomass,

133 value of $dE_o/dT = 0.022$ eV consistent with Deutsch et al. (2020). The Metabolic Index can thus
 134 be written as the ratio of S/D :

$$\begin{aligned}
 135 \quad \Phi &= \frac{\alpha_s B^\sigma}{\alpha_D B^\delta} pO_2 \exp\left\{\frac{-E_s}{K_B} \left[\frac{1}{T} - \frac{1}{T_{ref}}\right] + \frac{E_d}{K_B} \left[\frac{1}{T} - \frac{1}{T_{ref}}\right]\right\}, \\
 136 \quad &= A_o B^{\sigma-\delta} pO_2 \exp\left\{\frac{E_d - E_s}{K_B} \left[\frac{1}{T} - \frac{1}{T_{ref}}\right]\right\}, \\
 137 \quad &= A_o pO_2 \exp\left\{\frac{E_o}{K_B} \left[\frac{1}{T} - \frac{1}{T_{ref}}\right]\right\} \quad (3)
 \end{aligned}$$

138 where $A_o = \alpha_s/\alpha_D$ ($1/atm$) is the hypoxic tolerance, $E_o = E_d - E_s$ (E_s is the temperature
 139 dependence of oxygen supply) (Deutsch et al., 2015; Penn et al., 2018). The exponent, $\varepsilon = \sigma -$
 140 δ , is the allometric scaling of the supply to demand ratio with biomass, is typically near zero.
 141 Therefore, in the analysis that follows, we presume unit biomass and thus neglect potential
 142 impacts of variations in biomass.

143
 144 If Φ falls below a critical threshold value of 1, conditions are physiologically unsustainable: an
 145 organism cannot meet its basic resting metabolic oxygen requirements. Conversely, values of Φ
 146 above 1 enable organismal metabolic rates to increase by a factor of Φ above resting levels,
 147 permitting critical activities such as feeding, defence, growth, and reproduction. Thus, for a
 148 given environment and species, Φ provides an estimate of the ratio of maximum sustainable
 149 metabolic rate to the minimum rate necessary for basal metabolism. Deutsch et al. (2015)
 150 inferred the ratio of active to resting energetic demand by examining the biogeographic
 151 distribution of several species, finding that range boundaries coincide with values of $\Phi = 1.5-7$.
 152 This threshold, termed critical rate (Φ_{crit}), represents the minimum metabolic index required for
 153 an organism to sustain an active metabolic state, which is a more meaningful ecological
 154 threshold than requirements for resting metabolism. Therefore, in this study, we define a quantity

155 Φ' derived by dividing Φ by Φ_{crit} , so when Φ falls below 1, the organism can no longer sustain its
 156 active metabolic demand and will need to make physiological trade-offs. Account for these
 157 active metabolic requirements, we use an adjusted definition of the hypoxic tolerance trait, $A_c =$
 158 A_o / Φ_{crit} where A_c is termed the “ecological hypoxia tolerance”, consistent with Howard et al.,
 159 2020. Where $\Phi' > 1$ (i.e., $\Phi > \Phi_{crit}$) an organism can sustain an active metabolic rate; where $\Phi' <$
 160 1 (i.e., $\Phi < \Phi_{crit}$), O_2 is insufficient and an active metabolic state is not viable. Henceforth, our
 161 analysis focuses on Φ' ; in the subsequent $\Phi' = \Phi$ for the text and figures.

Formatted: Indent: First line: 1,27 cm
 Deleted: ¶
 Deleted: -
 Deleted: o
 Deleted: l
 Deleted: ¶

Formatted: Font: 12 pt
 Formatted: Font: 12 pt
 Formatted: Font: 12 pt
 Formatted: Font: 12 pt
 Deleted: Φ' , which is derived by dividing Φ by Φ_{crit} ; equivalently, this yields an adjusted definition of the hypoxic tolerance trait, $A_c = A_o / \Phi_{crit}$, where A_c is termed the “ecological hypoxia tolerance” consistent with Howard et al. (2020). ...
 Deleted: our analysis uses
 Deleted: to characterize ecotypes viability.

175

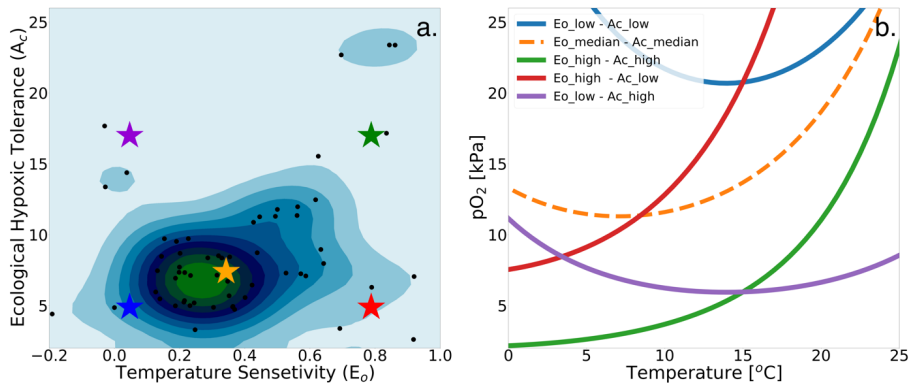
176 2.2 Physiological dataset

177 We make use of a dataset describing physiological parameters for a collection of 61 marine
178 ecotypes spanning a range of ecological hypoxic tolerances (A_c) and temperature sensitivities
179 (E_o) (Penn et al., 2018; Deutsch et al., 2020, Figure 1a). [The 61 species span benthic and pelagic](#)
180 [habitats across four phyla in all ocean basins \(Arthropoda, Chordata, Mollusca, and Cnidaria\).](#)
181 [The dataset include 28 malacostracans, 21 fishes, three bivalves and cephalopods, two copepods,](#)
182 [and one each for gastropods, ascidians, scleractinian corals, and sharks with body mass spans of](#)
183 [eight orders of magnitude \(Penn et al., 2018\).](#) We illustrate how the physiological traits E_o and A_c
184 constrain habitat viability in the context of distributions of pO_2 and temperature in the marine
185 environment in Figure 1b, which shows the minimum pO_2 (i.e., pO_2 at Φ_{crit}) required to sustain
186 an active metabolic state as a function of temperature for five combinations of E_o and A_c . The
187 five combinations are derived from sampling the probability distributions of E_o and A_c (Figure
188 1a) at the 10th, 50th, and 90th percentile values (illustrated by colored stars in Figure 1a and
189 corresponding curves in Figure 1b). We assume that the trait distributions are independent, which
190 is a reasonably modest simplification; E_o is represented by a normal distribution and A_c by a
191 lognormal distribution function (Figure S1). The pO_2 at Φ_{crit} curves shown in Figure 1b delineate
192 regions of pO_2 -temperature space that are habitable (above the curve) and uninhabitable (below
193 the curve). The reversing curvature of pO_2 at Φ_{crit} in Figure 1b at low temperature captures the
194 decrease of the organism's oxygen acquisition efficiency in cooler conditions yielding cold
195 intolerance. [At very low temperatures, gas transfer is limited by the decrease in molecular gas](#)
196 [diffusion, as a consequence, oxygen transfer into the organisms requires energy, yielding cold](#)

Deleted:

Formatted: Font: 12 pt

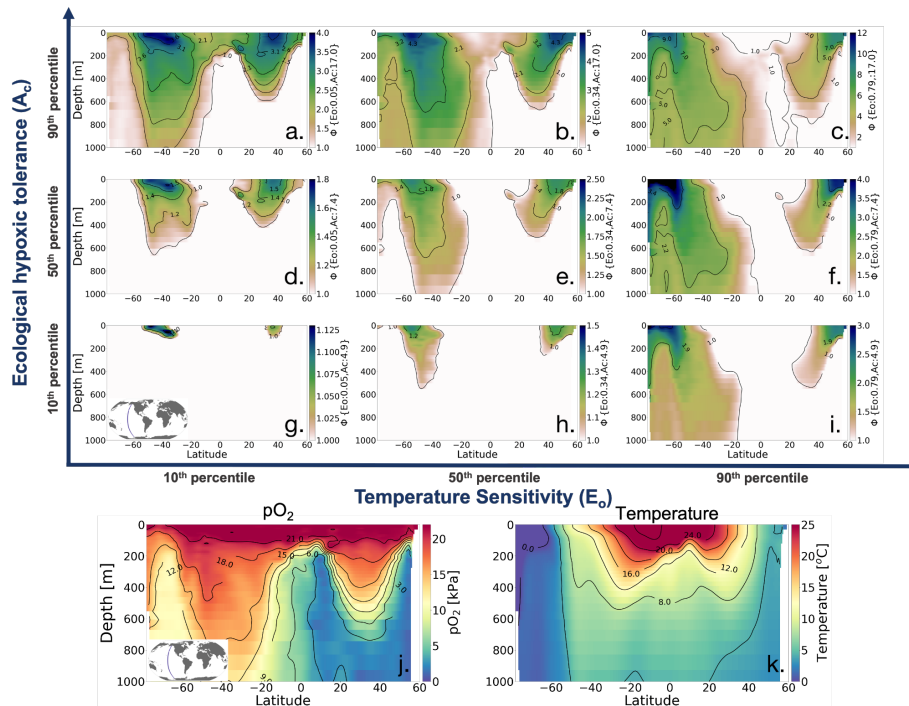
Formatted: Font: 12 pt



199
 200 **Figure 1.** Physiological traits determining hypoxic tolerance. (a) Scatter plot of 61 marine ecotypes for which
 201 empirically derived estimates of activation energy (E_o) and the ecological hypoxic tolerance (A_c) have been
 202 determined (Penn et al., 2018). The color shows the density of occurrence for the 61 marine ecotypes in the $A_c - E_o$
 203 trait space. (b) The minimum pO_2 required to sustain an active metabolic state (i.e., pO_2 at Φ_{crit} , Deutsch et al., 2020)
 204 for five combinations of A_c and E_o corresponding to the stars in panel “a”; these are combinations of the 10th, 50th,
 205 90th percentile values for each parameter.

206
 207 To illustrate how the trait combinations of E_o and A_c exert control on the geographic distribution
 208 of organisms in the marine environment (Deutsch et al., 2020), we use observations of pO_2 and T
 209 along a zonal transect of the Pacific Ocean and plot Φ' for nine combinations of E_o and A_c
 210 percentile values (Figure 2). The colorbar in Figures 2a-i show the metabolic index for an active
 211 state (Φ'); regions with values above one are habitable (color), while regions with values below
 212 one are uninhabitable (white) on the basis of metabolic constraints (other ecological
 213 considerations are not considered). The subplots in the upper portion of the figure are arranged
 214 according to the same trait axes shown in Figure 1a; E_o increases horizontally from left to right
 215 and A_c increases from the bottom to the top. For the trait combination in the bottom left (low E_o ,
 216 low A_c ; Figure 2g), metabolism is relatively insensitive to temperature, and tolerance for low
 217 pO_2 is poor. Thus, ecotypes with low E_o and low A_c are restricted to high latitude surface waters,
 218 where temperatures are cool, and pO_2 is abundant (Figure 2g). As E_o increases from left to right,
 219 metabolic rates become more sensitive to temperature. Then, habitat is gained at depth, where

220 temperatures are cooler and higher temperature sensitivity confers an advantage (Figure 2g–i).
 221 From the bottom to the top, the increase in tolerance of low pO_2 conditions increases habitability
 222 in regions of low pO_2 , enabling organisms to expand beyond high-latitude surface waters (Figure
 223 2g–a). The biogeographic range for organisms with high A_c is modulated by E_o ; as temperature
 224 sensitivity increases, ecotype viability at high latitudes is increased, but tropical surface waters
 225 become less viable (Figure 2 a–c). Henceforth, our analysis will utilize the metabolic index of the
 226 median ecotype ($E_o = 0.34$, $A_c = 7.4$; Figure 2e) for illustrative purposes; i.e., all metabolic index
 227 figures refer to this median ecotype unless otherwise stated.



228
 229 **Figure 2.** Annual mean metabolic index (Φ) for nine combinations of the ecological traits E_o (metabolic
 230 temperature sensitivity) and A_c (ecological hypoxic tolerance) along a transect in the Pacific Ocean based on a
 231 climatology from the World Ocean Atlas dataset (Garcia et al., 2014). The percentile values of each trait are: 10th (E_o
 232 = 0.04, $A_c = 4.8$), 50th ($E_o = 0.34$, $A_c = 7.4$), and 90th ($E_o = 0.79$, $A_c = 17.0$). The lower panels show pO_2 and
 233 temperature from the WOA dataset. Note that the colorbar range differs by panel and values where $\Phi < 1$ are
 234 omitted, thus the color shows only areas where an active metabolic state can be sustained.

235

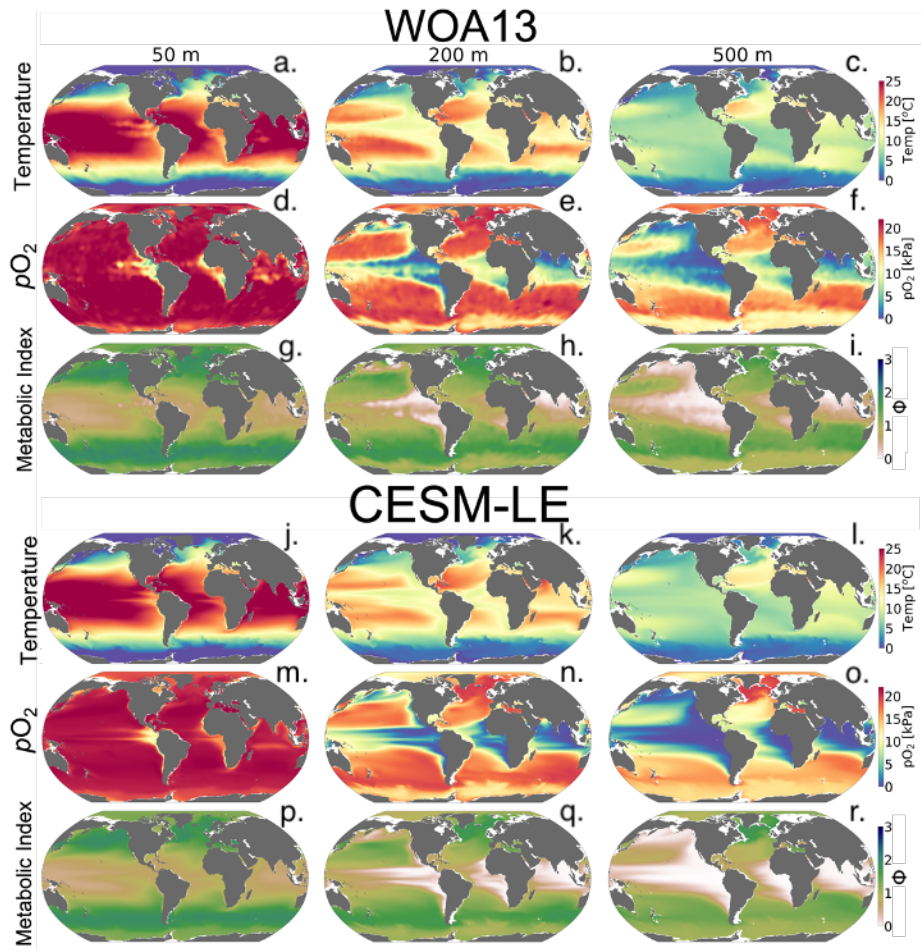
236 **2.3 Earth system model simulations**

237 This study is based on the CESM1-LE, described in detail by Kay et al. (2015). The CESM1-LE
238 included 34 ensemble members integrated from 1920–2100 under historical and RCP8.5 forcing.
239 The ensemble was generated by adding round-off level (10^{-14} K) perturbations to the air
240 temperature field at initialization in 1920; this small difference yields rapidly diverging model
241 solutions due to the chaotic dynamics intrinsic to the climate system, thus developing ensemble
242 spread representative of internal variability (Kay et al., 2015). Briefly, the CESM1-LE uses the
243 Community Earth System Model, version 1 (Hurrell et al., 2013), with a horizontal resolution of
244 nominally 1° in all components. The ocean component is Parallel Ocean Program version 2,
245 (Smith et al., 2010) with sea ice simulated by the Los Alamos Sea Ice Model version 4 (Hunke
246 and Lipscomb, 2010). Ocean biogeochemistry was represented by the Biogeochemical Elemental
247 Cycling (BEC) model (Moore et al., 2013; Lindsay et al., 2014).

248

249 Our analysis focuses on three depths: 50 m representing near-surface dynamics, the epipelagic
250 zone at 200 m, and the mesopelagic zone at 500 m. pO_2 was calculated using the Garcia and
251 Gordon. (1992) solubility formulation. For convenience, we use the period 1920–1965 to define
252 a minimally-perturbed natural state, as this period is prior to the development of substantial
253 anthropogenic trends in ocean oxygen and temperature (Long et al., 2016). We also examine
254 distributions over the last three decades of the 21st century (2070–2099) to evaluate the projected
255 climate-change signal under RCP8.5. We use the mean across all 34 ensemble members to
256 quantify the deterministic, “forced” response of the climate system to anthropogenic influence
257 (Deser et al., 2012). The ensemble spread is thus indicative of the amplitude of variations
258 attributable to natural variability.

259



260
 261 **Figure 3.** Mean-state comparison with observations. The climatological mean of (top rows) temperature (°C),
 262 (middle rows) pO_2 (kPa), and the (bottom rows) metabolic index for active metabolism (Φ') for the median ecotype
 263 ($E_o = 0.34$, $A_c = 7.4$); three depths are shown (left) 50 m, (center) 200 m, and (right) 500. Top panels show the
 264 WOA13 dataset and the bottom panels show CESM1-LE.

265
 266 We compared the CESM1-LE (1920 - 1965) with the World Ocean Atlas, version 2013
 267 (WOA2013) dataset (Garcia et al., 2014), an observationally-based, gridded climatology (Figure
 268 3a-i). CESM1-LE generally provides a reasonable representation of pO_2 and temperature

269 distributions at the selected depths (Figure 3); however, there are important biases to
270 acknowledge in the context of interpreting the results. Temperature magnitudes are generally
271 well simulated in the CESM1-LE, showing a root mean square error (RMSE) < 1.3 °C, and
272 pattern correlation coefficient (PCC) >0.98 in all three selected depths (50 m, 200 m, and 500)
273 (Table 1). Temperature magnitudes are slightly underestimated at 50 m and 200 m (mean bias of
274 < 0.3°C), and overestimated by 0.41 °C at 500 m. Note that since our comparison uses CESM1-
275 LE data from 1920-1965, some discrepancy in temperature might be expected from the signal of
276 climate warming present in the WOA observations. pO_2 is also reasonably well captured by the
277 CESM1-LE (PCC <0.95), but magnitudes are slightly underestimated at depth, showing a mean
278 bias of -1.63 kPa and -2.1 kPa at 200 m and 500 m with respect to WOA13 (Table 1). Regions of
279 low pO_2 waters are too extensive in CESM1-LE (Figure 3n-o) and there is a slight degradation of
280 skill with depth for pO_2 fields (Table 1). The underestimation of pO_2 leads to a slight
281 underestimation of Φ' with respect to WOA13, and overestimate habitat loss in the future
282 climate (Figure 3 p-r); however, Φ' computed from the model fields demonstrates that the
283 dominant spatial patterns are well captured by the CESM1-LE despite magnitudes that are
284 slightly too low (i.e., Figure 1, c, l). This CESM pO_2 bias is common among coarse-resolutions
285 ocean models and it is attributed to a sluggish circulation and hence weak ventilation (Long et
286 al., 2016). These differences ultimately matter most near the hypoxic zones and at the boundaries
287 of habitable zones like the Oxygen Minimum Zones (OMZs).

Deleted:

Deleted: OMZ

Deleted: s

288
289

293 **Table 1.** Summary statistics for the comparison of CESM1-LE with the World Ocean Atlas dataset (Garcia et al.,
 294 2014). The columns include the mean bias, pattern correlation coefficient (PCC), and root mean square error
 295 (RMSE) at 50 m, 200 m, and 500 m.

	Mean bias	R	RMSE
	Temperature [°C]		
50 m	-0.17	0.99	1.22
200 m	-0.25	0.99	1.22
500 m	0.10	0.98	0.63
	pO₂ [kPa]		
50 m	0.05	0.99	1.91
200 m	-1.17	0.96	5.96
500 m	-1.46	0.95	6.28
	Metabolic index		
50 m	0.01	0.99	0.02
200 m	-0.09	0.97	0.05
500 m	-0.15	0.96	0.08

296
 297

298 **2. Results**

299

300 **3.1 Joint temperature- pO_2 natural variability and forced trends**

301

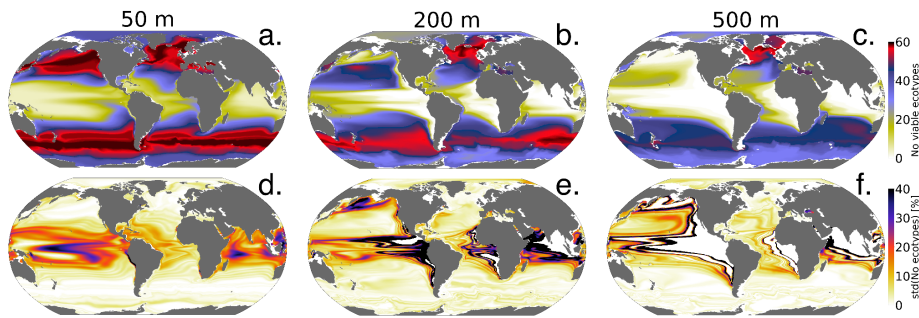
302 The spatial distribution of the number of viable ecotypes is shown in Figure 4 for the
303 “unperturbed” climate (1920-1965). Our intention here is not to quantify the actual
304 biogeographic range of organisms in the environment, but rather to illustrate the ocean’s ability
305 to support respiration by marine ectotherms given the metabolic capacities afforded within the
306 trait space of extant organisms. High latitude environments do not impose strong aerobic
307 constraints (cold intolerance notwithstanding), thus over much of the Southern Ocean, North
308 Atlantic, and Arctic Ocean almost all 61 ecotypes can sustain respiration. The tropical oceans
309 impose the strongest aerobic constraints, restricting the viability of ecotypes that do not have
310 high-hypoxia tolerance (A_o). For example, less than 25 ecotypes are viable over much of the
311 tropical surface ocean (Figure 4a); low concentrations of oxygen at depth impose even stronger
312 constraints, and no ecotypes are viable in the core of OMZs (Figure 4b, c). The spatial patterns of
313 the number of viable ecotypes is tightly controlled by temperature at the surface, since pO_2 is
314 mostly near saturated levels; at depth, however, pO_2 is the dominant driver of geographic
315 patterns in ecotype viability (Figures 2-4). Temperature generally decreases with depth, reducing
316 the metabolic oxygen demand. However, since pO_2 also decreases with depth and displays
317 greater lateral heterogeneity, pO_2 emerges as the dominant constraint of spatial structure in
318 ecotype viability at depth.

319

320 The standard deviation of annual anomalies using all CESM1-LE ensemble members provides
321 insight into the amplitude of natural variability (Figure. 5, [one standard deviation](#)). Temperature
322 and pO_2 show similar patterns of natural variability in the upper ocean, both showing particularly
323 large variance in the western tropical Pacific and Indian Ocean (Figure 5 a, d). Spatial variation
324 in the magnitude of temperature variability generally decreases with depth, but pO_2 displays even
325 relatively larger variability at depth with respect to the surface in some regions (Figure 5 a–f).

326 The joint pO_2 -temperature variability manifests in variations of Φ' (Figure 5g-i). Natural
327 variability in Φ' computed for the median ecotype shows spatial patterns similar to temperature

328 in the upper-surface ocean (50 m), but is more similar to pO_2 at depth. Thus, variations in Φ' tend
 329 to be temperature-dominated near the surface, but are more strongly controlled by pO_2 variability
 330 at depth. Φ' also shows the most extensive natural variability at 200 m consistent with the
 331 variability of pO_2 . The number of viable species shows more dramatic fluctuations than
 332 variations in the median ecotype Φ' ; variations in the number of viable ecotypes exceed 30% on
 333 annual timescales in the tropical upper ocean and near OMZ boundaries in the water column
 334 (Figure 4 c–d). This reflects the fact that interannual variability can preclude habitability for
 335 some regions of the A_c - E_o trait space, but these variations do not necessarily impact viability for
 336 the median ecotype (Figure 1). In the tropical surface ocean, high temperatures ($>25^\circ\text{C}$), and
 337 saturated surface ($pO_2 > 20$ kPa) require high hypoxia tolerance (A_c), but permit a range of
 338 E_o values (Figure 1b, 2a-b). Ecotypes with larger temperature sensitivity (high E_o) are
 339 particularly responsive to variations in temperature.
 340



341
 342 **Figure 4.** Metabolic constraints on trait-space viability. Top row: the number of ecotypes from the physiological
 343 trait database that are viable (total = 61) in the CESM1-LE over the period 1920–1965. Bottom row: the standard
 344 deviation (expressed as a percent of the mean) in the number of viable ecotypes, reflecting fluctuations driven by
 345 natural variability.
 346

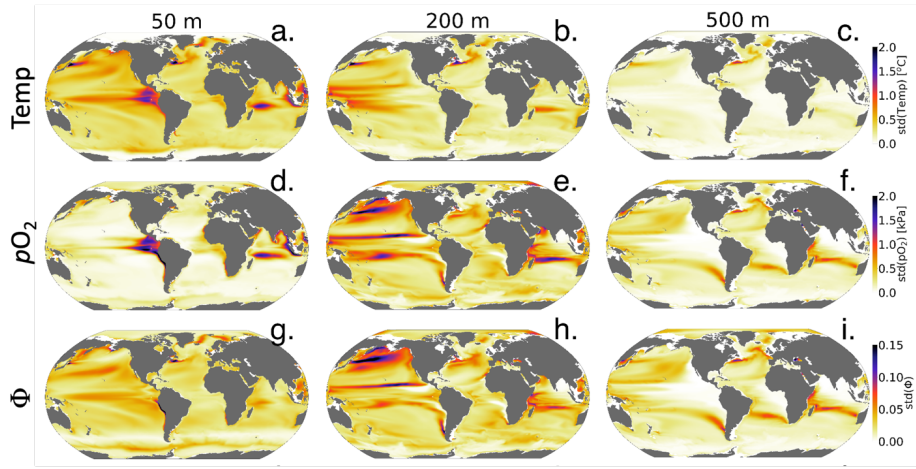
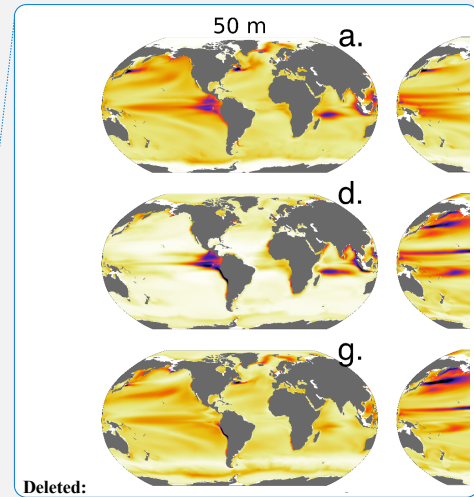


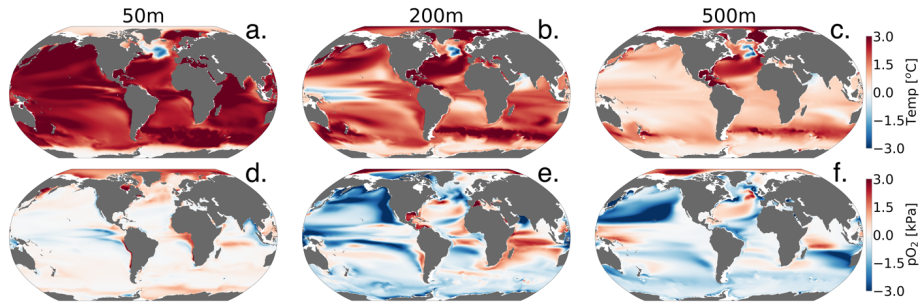
Figure 5. The amplitude of natural variability in the ocean’s metabolic state. The panels show the standard deviation of annual-mean anomalies of all ensemble members over the period 1920–1965 for (top row) temperature (°C), (middle row) pO_2 (kPa), and (bottom row) the metabolic index (unitless) of the median ecotype ($E_o = 0.34$, $A_c = 7.4$).

CESM1-LE simulates nearly homogeneous warming between 1920–1965 and 2070–2099 in the surface ocean (50 m) under RCP8.5, with an exception of the so-called North Atlantic warming hole (Figure 6a). Both modelling and observational studies have linked the North Atlantic warming hole to the slowing of the Atlantic overturning circulation with climate change (Keil et al., 2020). The magnitude of ocean warming generally diminishes with depth except in the North Atlantic, where, despite reductions, the overturning circulation effectively propagates anthropogenic heat anomalies into the ocean interior. pO_2 shows heterogeneous changes between 1920–1965 and 2070–2099 (Figure 6 d-f). In the upper ocean, pO_2 changes are generally small (< 1 kPa) because the near-surface is kept close to saturation via photosynthetic oxygen production and air-sea equilibration. At depth, however, pO_2 shows long-term changes linked to accumulated effects of respiration and changes in circulation (Ito et al., 2017). At 200 m for example, the Pacific Ocean displays a basin-wide mean reduction in pO_2 of 2 kPa (~30%), while the Atlantic and Indian basins gain about >2 kPa (~ 10 - 35%) by the end of the century. The largest long-term pO_2 loss (>3 kPa) occurs in the North Pacific while the largest pO_2 gain (~2



Deleted:

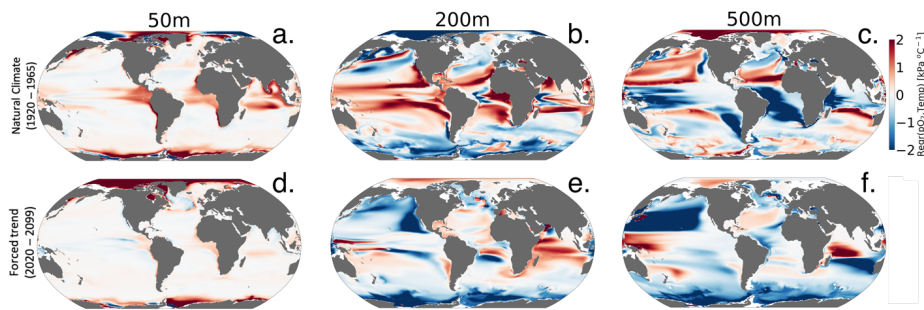
367 kPa) occurs in the North Atlantic gyre and western Indian Ocean (Figure 6 e-f).



368
369 **Figure 6.** Net long-term change (2070–2099 minus 1920–1965) in the CESM1-LE ensemble means temperature
370 (top) and (bottom) pO_2 at 50 m, 200 m, and 500 m.

371
372 Figure 7 shows the relationship between interannual variations in pO_2 versus temperature (pO_2 -
373 T) in the unperturbed climate (1920–1965; top row) and for the forced trend associated with 21st
374 century climate change (2070–2099 minus 1920–1965; bottom row). The nature of the pO_2 -T
375 relationship is an important indicator of the impacts of variability on the metabolic state.
376 Furthermore, the extent to which the forced trend is characterized by a pO_2 -T relationship that is
377 distinct from that associated with natural variability provides insight into the potential for
378 advanced or delayed detection of signals in Φ relative to pO_2 or temperature alone. Given that
379 metabolic rates for most organisms increase with temperature (positive E_o), a positive correlation
380 between variations in temperature and pO_2 is generally indicative of compensating changes,
381 wherein increased oxygen demand is at least partially offset by increased supply. Anticorrelation
382 between temperature and pO_2 , by contrast, will generally be associated with compounding
383 impacts on the metabolic index, as a negative correlation indicates that reductions in pO_2 (i.e.,
384 oxygen supply) accompany warming (i.e., increased demand). The sign of the pO_2 -T relationship
385 in the natural climate varies regionally and with depth (Figure 7, top row). The surface ocean is
386 generally characterized by a weak, positive pO_2 -T relationship, which could manifest from,
387 among other mechanisms, temperature-induced increases in photosynthetic oxygen production
388 (Figure 7a). The natural pO_2 -T relationship in the epipelagic (200 m) is characterized by strong
389 positive correlations in the tropics and negative correlations at high latitudes (Figure 7b). A
390 positive correlation between pO_2 and temperature at this depth could be induced by variability

391 associated with adiabatic vertical displacement of isopycnals, or “heave”, which has the effect of
 392 translating background gradients in properties vertically in the water column (Long et al., 2016).
 393 Upward movement of a deep isopycnal surface would yield a negative temperature anomaly and
 394 a negative pO_2 anomaly (positive correlation), as the deeper, colder waters have greater oxygen
 395 utilization signatures associated with longer ventilation age. Negative correlations between pO_2
 396 and temperature could manifest from ventilation processes, where enhanced subduction of
 397 surface water yields anomalously cold water masses that are enriched in oxygen. The sign of
 398 these epipelagic pO_2 -T correlations shows some similarity to those associated with the externally
 399 forced climate (Figure 6e), but the latter is characterized by a greater prevalence of
 400 anticorrelation, most notably in the North Pacific ocean. At 500 m depth, the relationship
 401 between temperature and pO_2 in the natural climate is almost a mirror image of the epipelagic
 402 (Figure 7c); the tropics generally display negative correlations, while polar regions show positive
 403 correlations (Figure 7 e). The pO_2 -T relationship in the forced trend at 500 m is dominated by
 404 broad regions of deeply negative correlations, with the most pronounced effect again in the
 405 North Pacific. The negative relationship is consistent with a ventilation signal, as buoyancy-
 406 induced stratification from warming curtails the introduction of new oxygen into the ocean
 407 interior. The predominantly negative pO_2 -T relationship associated with the forced trend is
 408 indicative of the compounding effects of climate change on metabolic state, increasing metabolic
 409 demand while simultaneously reducing oxygen supply.



410
 411 **Figure 7.** Regression of annual means pO_2 versus temperature ($kPa \cdot ^\circ C^{-1}$) for (top row) interannual variability and
 412 (bottom row) the forced trend (difference between 2020–2099 and 1920–1965). The columns show the regressions
 413 computed at different depths, 50 m, 200 m, and 500 m, respectively.
 414

3.2 Long-term habitat changes

Figure 8 shows the climate-driven changes in Φ' for the median ecotype, as well as the impacts of climate change on the number of viable ecotypes. Notably, while pO_2 in the near-surface ocean is relatively insensitive to climate change (Figure 6d), there are reductions in Φ' in the tropics (Figure 9d), owing to the direct impacts of warming. These changes are associated with deep reductions in the number of viable ecotypes in the tropics (Figure 8a). There are modest increases in Φ' and ecotype viability at high-latitudes; metabolic state in these regions is affected by cold intolerance, thus warming broadens the viable region of trait space. Additionally, reductions in sea ice cause an increase in pO_2 , as gas exchange becomes more effective at restoring equilibrium oxygen concentrations. The number of viable ecotypes shows more intense patterns than those in the median ecotype Φ' in the upper ocean (Figure 8). This is partly because ecotypes predicted to lose viability in the tropical regions ($\sim 50\%$) are at the extremes of the A_c - E_o distribution (Figure 1) and not captured by the median ecotype Φ' . Nevertheless, outside the tropical regions, the median ecotype gives a good indication of the anthropogenic impact to marine ectotherms. The projected habitat loss in the epipelagic-pelagic North Pacific ($> 50\%$) and habitat gain in the epipelagic-pelagic Southern Indian Ocean ($\sim 40\%$) and pelagic western tropical regions ($\sim 40\%$) are consistent with a decrease in the median ecotype Φ' . Note that the most pronounced effects on habitat are associated with regions where climate change drives a strongly negative pO_2 -temperature relationship (Figure 7).

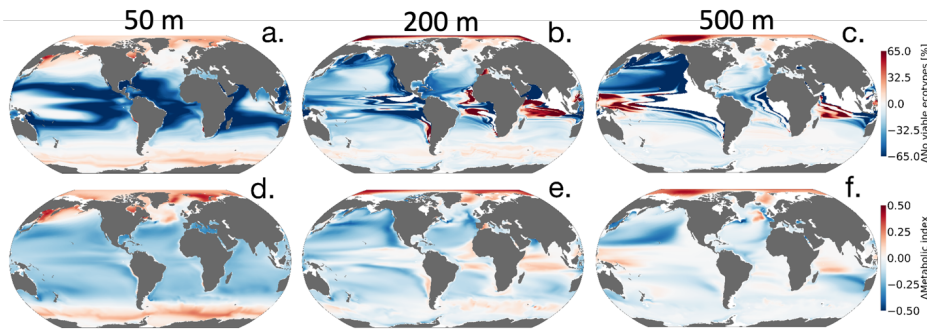
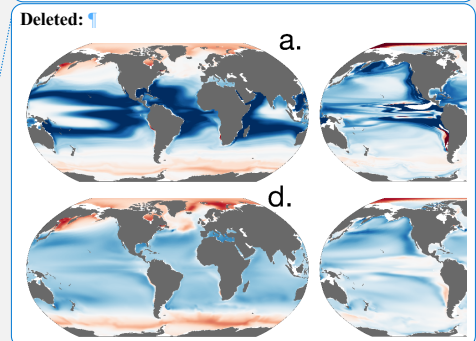
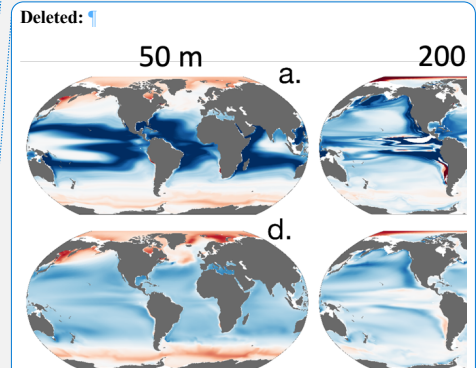


Figure 8. Net change in the number of habitable ecotypes in percentage (top row). Net metabolic index change

Formatted: Pattern: Clear (White), Tab stops: 1,62 cm, Left + 3,23 cm, Left + 4,85 cm, Left + 6,46 cm, Left + 8,08 cm, Left + 9,69 cm, Left + 11,31 cm, Left + 12,92 cm, Left + 14,54 cm, Left + 16,16 cm, Left + 17,77 cm, Left + 19,39 cm, Left + 21 cm, Left + 22,62 cm, Left + 24,23 cm, Left + 25,85 cm, Left



441 (2070 - 2099 vs. 1920 - 1965) for the median ecotype [$E_o = 0.34$, $A_e = 7.4$] (bottom row). At 50m (first column),
442 200m (second column) and 500m (third column).

443

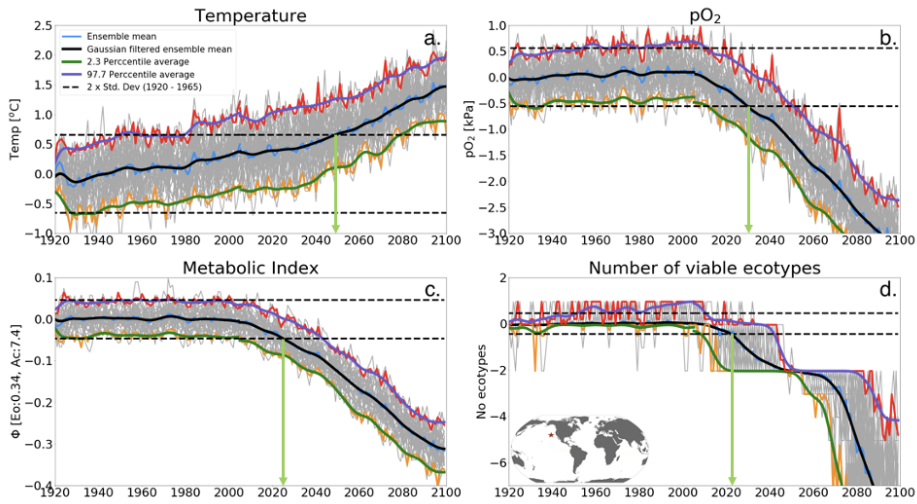
444 3.3 Time of Emergence

445

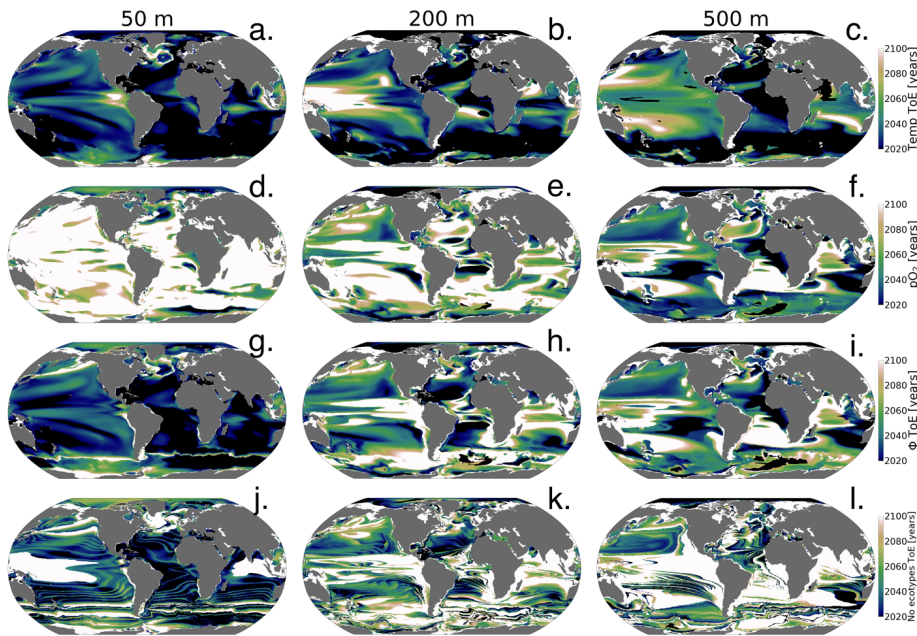
446 In this section, we examine the “time of emergence” (ToE, Hawkins and Sutton, 2012), the point
447 when forced changes in pO_2 , temperature and Φ' can be distinguished from the background
448 natural variability. We define ToE as the time when the magnitude of change in the ensemble
449 mean of a particular variable exceeds two standard deviations of the natural climate (1920 -
450 1965). This is illustrated in Figure 9 for a single grid point in the North Pacific at 200 m. At this
451 location, the forced trend in temperature shows a monotonic increase, while pO_2 shows a
452 monotonic decrease; as a result, Φ' for the median ecotype and the number of viable ecotypes
453 decrease over time. The anti-correlation between pO_2 and temperature exacerbates trends in Φ' ,
454 and hence the forced trend of the median ecotype Φ' emerges from natural noise earlier than
455 either pO_2 or temperature do alone (Figure 10a-c). Note that although the ToE of ecotype
456 viability change is directly derived from changes in Φ' , it is binary counted; changes in ecotype
457 viability are counted in whole numbers and this creates a step-function temporal-spatial variation
458 (Figure 9d). Consequently, this step-function-like feature of ecotype viability creates
459 discontinuities even in spatial patterns of ToE (Figure 10 j-l) as also shown in the natural
460 variance in Figure 4 d-f.

461

462



463
 464 **Figure 9.** Time of emergence (ToE) of the climate forcing signal for (a) temperature, (b) pO₂ (c) the metabolic
 465 index of the median ecotype [$E_o = 0.34$, $A_c = 7.4$], and (d) the number of viable ecotypes for a single model grid in
 466 the North Pacific at 200 m. ToE (green arrows) is defined as the time when the forced trend signal (ensemble
 467 member time series) is above two standard deviations (black dotted line) of all ensemble members for the period
 468 1920 - 1965.
 469



470
 471 **Figure 10.** Time of emergence (ToE) of the climate forcing signal for temperature, pO_2 , ϕ , and the number of
 472 viable ecotypes. ToE is defined as the time when the forced trend signal (ensemble member time series) is above
 473 two standard deviations of all ensemble members for the period 1920 - 1965.

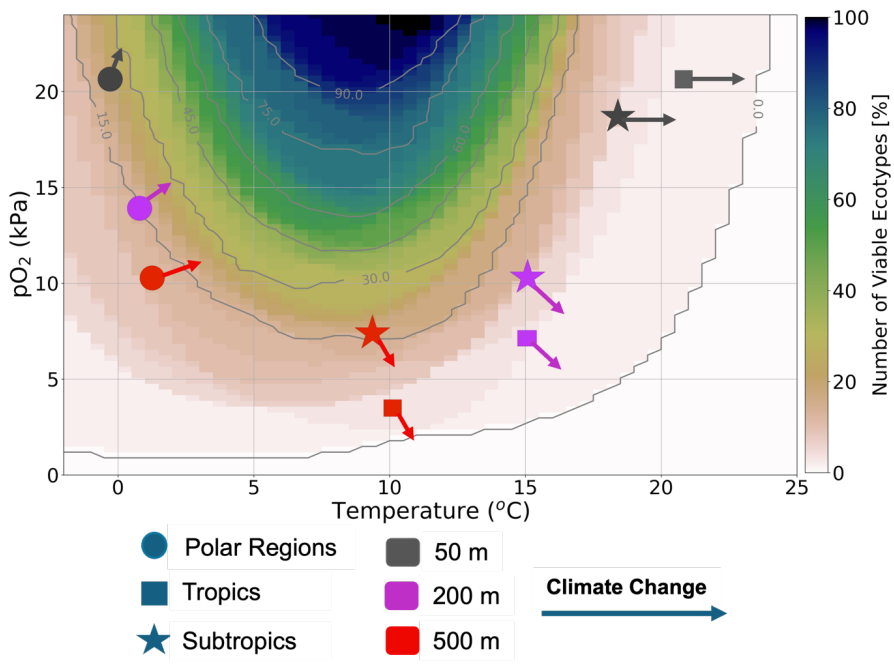
474
 475 The ToE of pO_2 and temperature are inverted with depth; temperature emerges earliest in the
 476 upper ocean while pO_2 emerges earlier at depth and later or shows no emergence in the upper
 477 ocean (Figure 10 a-f). This feature is consistent with larger upper ocean temperatures long-term
 478 changes and greater pO_2 changes at depth. Near-surface ocean temperature has mostly already
 479 emerged by 2020 and is predicted to have almost completely emerged by the late 2060s under
 480 RCP85 (Figure 10 a-c). The early emergence of temperature from natural noise also persists for
 481 regions of relatively low natural variance at depth, e.g., the Southern Ocean and Atlantic Basin
 482 Gyres. Regions of the largest natural variability (see Figure 5) like the subtropical-subpolar
 483 Pacific however do not emerge until close to the end of the century. For pO_2 , anthropogenic
 484 changes in the upper ocean generally do not emerge from natural noise before the end of the
 485 century except for the Arctic Ocean and Eastern Antarctic. In the Arctic Ocean and Eastern

486 Antarctic pO_2 gain is related to sea-melt emergence by the mid-2050s (Figure 10a). The median
487 ecotype Φ' ToE shows spatial patterns that are coherent with temperature ToE in the upper ocean
488 with exception of polar regions. In contrast, they are consistent with pO_2 ToE patterns at depth;
489 this is consistent with net long-term Φ' changes in Figure 9d. The emergence of the
490 anthropogenic signal in ecotype viability closely resembles the median ecotype Φ' spatial
491 patterns but showing non-harmonious spatial patterns due to the step-function-like counting
492 feature of viability changes. It shows that the predicted ~ 50% ecotype viability loss in the
493 tropics (Figure 6a) may already be distinguishable from natural variability by the mid-2030s. In
494 the North Pacific, the predicted > 50% ecotype viability loss in the epipelagic-pelagic regions is
495 predicted to start emerging in the 2040s at 500 m and 2080s at 200 m (Figure 10 k-l).

496
497 In summary, we showed that because of the surface ocean's large warming signal and the least
498 pO_2 loss outside of the polar regions under the RCP85 climate scenario, it is characterized by
499 habitat loss in the tropics and a slight habitat gain in polar regions (Figure 11). Sea-ice melts
500 support Oxygen gain through the enhancement of temperature-driven solubility in the surface
501 polar regions. At depth, warming is less prevalent by the end of the 21st century; however,
502 oxygen loss related to the weakening ventilation of the ocean interior as the ocean becomes more
503 stratified has a stronger impact on metabolic reliance, leading to habitat loss in tropics and
504 subtropics. On the other hand, cooler temperatures and efficient ventilation in polar regions
505 create an oxygen-rich environment. Thus, in contrast to tropical and subtropical regions,
506 warming leads to a slight habitat gain (Figure 11), as organisms escape the cold intolerance
507 imposed by molecular gas diffusion at low temperatures.

Formatted: Font: Italic

Formatted: Subscript



508 **Figure 11, Summary Figure:** It shows the distribution of ecotype viability within representative ocean temperature and pO_2 boundaries for the 66 species analysed in this study. The markers represent the subsampled regions, with polar regions denoted by circles, tropical regions by squares, and subtropical regions by stars. The colours represent the depth levels; 50 m (grey), 200 m (purple), and 500 m (red). Each arrow shows the estimated joint temperature- pO_2 climate change vector based on the net changes in temperature and pO_2 (as depicted in Figure 6).

515 **4. Discussion**

516 The human-induced rapid warming of the planet has been shown to drive ocean deoxygenation
 517 (Ito et al., 2017; Schmidtko et al., 2017; Long et al., 2016). Higher metabolic oxygen demand at
 518 higher temperatures (Gillooly et al., 2001; Deutsch et al., 2015, 2022) raises concerns about the
 519 ability of marine ectotherms to support aerobic respiration in the future. This study set out to
 520 characterize the anticipated climate change signal in the ocean's metabolic state in the context of
 521

- Deleted: ¶
- Formatted: Font: 10 pt, Bold
- Formatted: Font: 10 pt
- Formatted: Font: 10 pt
- Formatted: Font: 10 pt, Italic
- Formatted: Font: 10 pt
- Formatted: Font: 10 pt, Subscript
- Formatted: Font: 10 pt
- Formatted: Font: 10 pt
- Formatted: Font: 10 pt
- Formatted: Font: 10 pt, Italic
- Formatted: Font: 10 pt
- Formatted: Font: 10 pt, Subscript
- Formatted: Font: 10 pt
- Formatted: Font: 10 pt, Italic
- Formatted: Font: 10 pt
- Formatted: Font: 10 pt, Subscript
- Formatted: Font: 10 pt
- Formatted: Font: 10 pt

523 natural variability using the metabolic theory as a basis to examine the capacity of the
524 environment to support ectothermic marine heterotrophs.

525
526 The spatial variation in pO_2 and temperature in the unperturbed natural climate state set
527 biogeographic boundaries based on ectotherms' physiological performance. The resilience of
528 these ectotherms' biogeographic structure to natural variability and long-term climate warming is
529 perturbed by the joint pO_2 -temperature changes, effectively measured by the metabolic index
530 (Φ). An increase in the capacity of the organisms to support aerobic respiration increases Φ ; for
531 example by ocean cooling or increase in oxygen supply contrary, warming and decrease in
532 oxygen supply decrease Φ . There are exceptions in extremely low-temperature environments
533 (Figure 11), where aerobic respiration is also limited by kinematic gas transfer into the organism
534 in addition to environmental oxygen supply. Relative changes in pO_2 and temperature in the
535 natural variability and forced trend, therefore, regulate ectotherms' resilience to environmental
536 changes. Under the RCP85 climate scenario, the ocean generally warms homogeneously but
537 concurrent pO_2 changes are heterogeneous and vary with depth. Thus, the characteristics of these
538 pO_2 -temperature forced trend changes determine when the climate change impact on marine
539 ectotherms can be distinguishable from natural variability.

540
541 In the surface ocean, pO_2 is generally abundant and relatively uniform, and thus spatial
542 temperature variations have a dominant constraint on the spatial variations of organismic
543 metabolic state. The warmest parts of the surface ocean, the tropical oceans, can only support
544 about 10-20 (~ 30%) of the 61 ecotypes while cooler regions in extratropics have nearly 100%
545 viability. Moreover, since warming anomalies propagate from the surface, the surface tropical
546 oceans also show the largest natural variance in temperature and ecotype viability. This is
547 because extremely warm temperatures in the surface tropics (>25°C) are mainly suited for
548 organisms with high-temperature sensitivity (E_o), which are relatively fewer, and mostly close to
549 their physiological limits (Storch et al., 2014). Large natural variability in these warmest parts of
550 the tropical surface ocean precludes the forced trend signal from emerging from the natural
551 variability in the ecotype viability by end of the century although the ocean warms the largest in
552 the surface. Nevertheless, the large warming trends in the surface ocean generally emerge
553 relatively early (the 2020s) from natural variability in both temperature and ecotype viability in

Deleted: in the surface ocean.

555 most regions. Minimal changes in surface pO_2 in the forced trend affirm that surface ocean
556 marine ectotherms are mainly perturbed by temperature in the context of anthropogenic changes.
557 In polar regions, warming has a counterintuitive effect on marine ectotherms with respect to
558 most parts of the surface ocean. There, warming helps organisms escape extreme cold
559 intolerances by enhancing membrane kinematic gas transfer which enhances Φ' and thus ecotype
560 richness in the future (Figure 11).

561
562 In the epipelagic and mesopelagic regions (200 m and 500 m), the forced temperature trend and
563 natural variability are broadly smaller than the surface ocean, while pO_2 changes show the
564 opposite. Thus, at depth pO_2 play a more intricate role in perturbing marine ectotherm habitats
565 in the context of anthropogenic warming with respect to the surface ocean, where temperature
566 plays a dominant role. Contrasting the regression between pO_2 and temperature in the natural
567 climate, and forced trends provides an instructive framework to analysing ectotherms' long-term
568 changes. Regions showing different correlations between temperature and pO_2 in the forced
569 trends in comparison to the natural climate suggest a loss metabolic resilience; loss of habitat,
570 and these regions tend to have a relatively early ToE. For instance, in the epipelagic and
571 mesopelagic North Pacific, temperature- pO_2 regressions switched from a positive correlation in
572 the unperturbed climate to a strong negative correlation in the forced trend (Figure 7). The North
573 Pacific pelagic – epipelagic regions is projected to lose nearly half of the present climate ecotype
574 viability by end of the 21st century, the projected habitat loss start emerging by the late 2030s
575 under the RCP85 climate scenario. On the other hand, in the Arctic Ocean and some parts of the
576 Southern Ocean, same sign pO_2 -temperature correlations in the forced trends result in the
577 preservation of the marine habitat and even slight enhancements.

579 5. Conclusions

580
581 The joint temperature-oxygen metabolic framework in this study provides additional insight into
582 the impact of climate change on marine ecosystems in comparison to the independent oxygen or
583 temperature analysis. We here showed that while warming is the leading order driving
584 mechanism of climate change, the direct effect of warming on marine ecosystems is mostly in

Deleted: .

Deleted: forced

Deleted: are

Deleted: compared to

Deleted: concurrent

Deleted: are larger than the surface ocean

Deleted: and temperature

Deleted: At depth, c

Deleted: analyzing

Deleted: distinct

Deleted: relative

Deleted: variability

Deleted: show a weakening

Deleted:

Deleted: and emerging relatively early from natural variability

Deleted: example

Deleted: pelagic - epipelagic

Deleted: Consequently, the pelagic-epipelagic North Pacific

Deleted: by the end of the century. This

Deleted: of pelagic - epipelagic North Pacific habitat is projected to emerge

Deleted: earliest at 500 m (

Formatted: Superscript

Deleted:)

Deleted: where anthropogenic pO_2 losses are larger than at 200 m.

Deleted: concomitant

612 the upper ocean. Climate change-related oxygen loss is a major driver of marine ecosystem stress
613 in addition to warming at depth. Incorporating organismal physiological sensitivity to oxygen-
614 temperature changes in the metabolic framework provides insight into how climate impacts the
615 biogeographic structure of marine habitat. [We find that forced perturbations to pO₂ and](#)
616 [temperature will strongly exceed those associated with the natural system](#) in many parts of the
617 upper ocean, mostly pushing organisms in these environments closer to or beyond their
618 physiological limits. Climate warming is expected to drive significant marine habitat loss in the
619 surface tropical oceans and epipelagic - pelagic North Pacific Basin, while gaining marginal
620 habitat viability in the surface Arctic Ocean and some parts of the Ocean Southern.

Formatted: Subscript

Deleted: We find that underway forced trends perturbations in pO₂ and temperature will strongly exceed those associated with the natural system

621

6. Competing interests

622 The contact author has declared that none of the authors has any competing interests

624

7. Acknowledgments

626

627 PM, ML, CD and TI were funded by the National Science Foundation (NSF) grant agreement
628 No. 1737158. PM and YSF were also funded by the European Union's Horizon 2020 research
629 and innovation programme under grant agreement No. 820989 (COMFORT).). We also would
630 like to acknowledge the data access and computing support provided by the NCAR Cheyenne
631 HPC.

8. Author contribution

633

634 PM and ML designed the study approach. PM developed the analysis with feedback from ML,
635 CD and TI. PM prepared the manuscript with contributions from all co-authors.

Deleted: model code and

636

9. Data access

638

639 The CESM1 large ensemble data used in this study can be accessed in this location:

640 <https://www.cesm.ucar.edu/community-projects/lens/data-sets>

641

646 **10. References**

647

648 Breitburg, D., Levin, L. A., Oschlies, A., Grégoire, M., Chavez, F. P., Conley, D. J., Garçon, V.,
649 Gilbert, D., Gutiérrez, D., Isensee, K., Jacinto, G. S., Limburg, K. E., Montes, I., Naqvi, S. W.
650 A., Pitcher, G. C., Rabalais, N. N., Roman, M. R., Rose, K. A., Seibel, B. A., Telszewski, M.,
651 Yasuhara, M., and Zhang, J.: Declining oxygen in the global ocean and coastal waters,
652 <https://doi.org/10.1126/science.aam7240>, 5 January 2018.

653

654 Deser, C., Phillips, A., Bourdette, V., and Teng, H.: Uncertainty in climate change projections:
655 The role of internal variability, *Clim Dyn*, 38, 527–546, [https://doi.org/10.1007/s00382-010-](https://doi.org/10.1007/s00382-010-0977-x)
656 [0977-x](https://doi.org/10.1007/s00382-010-0977-x), 2012.

657

658 Deutsch, C., Ferrel, A., Seibel, B., Pörtner, H. O., and Huey, R. B.: Climate change tightens a
659 metabolic constraint on marine habitats, *Science* (1979), 348, 1132–1135,
660 <https://doi.org/10.1126/science.aaa1605>, 2015.

661

662 Deutsch, C., Penn, J. L., and Seibel, B.: Metabolic trait diversity shapes marine biogeography,
663 *Nature*, 585, 557–562, <https://doi.org/10.1038/s41586-020-2721-y>, 2020.

664

665 Deutsch, C., Penn, J. L., Verberk, W. C. E. P., Inomura, K., Endress, M.-G., and Payne, J. L.:
666 Impact of warming on aquatic body sizes explained by metabolic scaling from microbes to
667 macrofauna, <https://doi.org/10.1073/pnas>, 2022.

668

669 Garcia, H. E. and Gordon, L. I.: Oxygen solubility in seawater: Better fitting equations,
670 <https://doi.org/10.4319/lo.1992.37.6.1307>, 1992.

671

672 Garcia, H. E. , Boyer, T. P. , Locarnini, R. A. , Antonov, J. I. , Mishonov, A. V. , Baranova, O.
673 K. , Melissa, M. Z. , Reagan, J. R. , and Johnson, D. R. .: WORLD OCEAN ATLAS 2013
674 Volume 3: Dissolved Oxygen, Apparent Oxygen Utilization, and Oxygen Saturation, 75,
675 <https://doi.org/10.7289/V5XG9P2W>, 2014.

676

677 Gillooly, J., Brown, J., West, G., Savage, V., Charnov, E., Gillooly, J. F., Brown, J. H., West, G.
678 B., Savage, V. M., and Charnov, E. L.: Effects of size and temperature on metabolic rate
679 Recommended Citation, 2001.

680

681 Hawkins, E. and Sutton, R.: Time of emergence of climate signals, *Geophys Res Lett*, 39,
682 <https://doi.org/10.1029/2011GL050087>, 2012.

683

684 Hoegh-Guldberg, O. and Bruno, J. F.: The Impact of Climate Change on the World's Marine
685 Ecosystems, *New Series*, 328, 1523–1528, <https://doi.org/10.1126/science.1185779>, 2010.

686 Howard, E. M., Penn, J. L., Frenzel, H., Seibel, B. A., Bianchi, D., Renault, L., Kessouri, F.,
687 Sutula, M. A., McWilliams, J. C., and Deutsch, C.: Climate-driven aerobic habitat loss in the
688 California Current System, 2020.

689

690 Hunke, E. C. and Lipscomb, W. H.: CICE: the Los Alamos Sea Ice Model Documentation and
691 Software User's Manual Version 4.1 LA-CC-06-012, 2010.

692

693 Hurrell, J. W., Holland, M. M., Gent, P. R., Ghan, S., Kay, J. E., Kushner, P. J., Lamarque, J. F.,
694 Large, W. G., Lawrence, D., Lindsay, K., Lipscomb, W. H., Long, M. C., Mahowald, N., Marsh,
695 D. R., Neale, R. B., Rasch, P., Vavrus, S., Vertenstein, M., Bader, D., Collins, W. D., Hack, J. J.,
696 Kiehl, J., and Marshall, S.: The community earth system model: A framework for collaborative
697 research, *Bull Am Meteorol Soc*, 94, 1339–1360, <https://doi.org/10.1175/BAMS-D-12-00121.1>,
698 2013.

699

700 Ito, T. and Deutsch, C.: A conceptual model for the temporal spectrum of oceanic oxygen
701 variability, *Geophys Res Lett*, 37, <https://doi.org/10.1029/2009GL041595>, 2010.

702

703 Ito, T., Minobe, S., Long, M. C., and Deutsch, C.: Upper ocean O₂ trends: 1958–2015, *Geophys*
704 *Res Lett*, 44, 4214–4223, <https://doi.org/10.1002/2017GL073613>, 2017.

705

706 Kay, J. E., Deser, C., Phillips, A., Mai, A., Hannay, C., Strand, G., Arblaster, J. M., Bates, S. C.,
707 Danabasoglu, G., Edwards, J., Holland, M., Kushner, P., Lamarque, J. F., Lawrence, D.,
708 Lindsay, K., Middleton, A., Munoz, E., Neale, R., Oleson, K., Polvani, L., and Vertenstein, M.:
709 The community earth system model (CESM) large ensemble project: A community resource for
710 studying climate change in the presence of internal climate variability, *Bull Am Meteorol Soc*,
711 96, 1333–1349, <https://doi.org/10.1175/BAMS-D-13-00255.1>, 2015.

712

713 Keeling, R. F., Körtzinger, A., and Gruber, N.: Ocean deoxygenation in a warming world, *Ann*
714 *Rev Mar Sci*, 2, 199–229, <https://doi.org/10.1146/annurev.marine.010908.163855>, 2010.

715 Keil, P., Mauritsen, T., Jungclaus, J., Hedemann, C., Olonscheck, D., and Ghosh, R.: Multiple
716 drivers of the North Atlantic warming hole, *Nat Clim Chang*, 10, 667–671,
717 <https://doi.org/10.1038/s41558-020-0819-8>, 2020.

718

719 Lindsay, K., Bonan, G. B., Doney, S. C., Hoffman, F. M., Lawrence, D. M., Long, M. C.,
720 Mahowald, N. M., Moore, J. K., Randerson, J. T., and Thornton, P. E.: Preindustrial-control and
721 twentieth-century carbon cycle experiments with the Earth system model CESM1(BGC), *J Clim*,
722 27, 8981–9005, <https://doi.org/10.1175/JCLI-D-12-00565.1>, 2014.

723

724 Long, M. C., Deutsch, C., and Ito, T.: Finding forced trends in oceanic oxygen, *Global*
725 *Biogeochem Cycles*, 30, 381–397, <https://doi.org/10.1002/2015GB005310>, 2016.

726

727 Moore, J. K., Lindsay, K., Doney, S. C., Long, M. C., and Misumi, K.: Marine ecosystem
728 dynamics and biogeochemical cycling in the community earth system model [CESM1(BGC)]:
729 Comparison of the 1990s with the 2090s under the RCP4.5 and RCP8.5 scenarios, *J Clim*, 26,
730 9291–9312, <https://doi.org/10.1175/JCLI-D-12-00566.1>, 2013.

731

732 Oeschlies, A., Brandt, P., Stramma, L., and Schmidtko, S.: Drivers and mechanisms of ocean
733 deoxygenation, <https://doi.org/10.1038/s41561-018-0152-2>, 1 July 2018.

734

735 Penn, J. L., Deutsch, C., Payne, J. L., and Sperling, E. A.: Temperature-dependent hypoxia
736 explains biogeography and severity of end-Permian marine mass extinction, *Science* (1979), 362,
737 <https://doi.org/10.1126/science.aat1327>, 2018.

738

739 Piiper, J., Dejours', P., Haab, P., and Rahn, H.: CONCEPTS AND BASIC QUANTITIES IN
740 GAS EXCHANGE PHYSIOLOGY, *Respiration Physiology*, 292–304 pp., 1971.

741 Portner, H. O.: Climate variations and the physiological basis of temperature dependent
742 biogeography: systemic to molecular hierarchy of thermal tolerance in animals, *Comparative*
743 *Biochemistry and Physiology Part A*, 739–761 pp., 2002.

744

745 Pozo Buil, M. and Di Lorenzo, E.: Decadal dynamics and predictability of oxygen and
746 subsurface tracers in the California Current System, *Geophys Res Lett*, 44, 4204–4213,
747 <https://doi.org/10.1002/2017GL072931>, 2017.

748

749 Rodgers, K. B., Lin, J., and Frölicher, T. L.: Emergence of multiple ocean ecosystem drivers in a
750 large ensemble suite with an Earth system model, *Biogeosciences*, 12, 3301–3320,
751 <https://doi.org/10.5194/bg-12-3301-2015>, 2015.

752

753 Rosewarne, P. J., Wilson, J. M., and Svendsen, J. C.: Measuring maximum and standard
754 metabolic rates using intermittent-flow respirometry: A student laboratory investigation of
755 aerobic metabolic scope and environmental hypoxia in aquatic breathers, *J Fish Biol*, 88, 265–
756 283, <https://doi.org/10.1111/jfb.12795>, 2016.

757

758 Schlunegger, S., Rodgers, K. B., Sarmiento, J. L., Frölicher, T. L., Dunne, J. P., Ishii, M., and
759 Slater, R.: Emergence of anthropogenic signals in the ocean carbon cycle, *Nat Clim Chang*, 9,
760 719–725, <https://doi.org/10.1038/s41558-019-0553-2>, 2019.

761

762 Schmidtko, S., Stramma, L., and Visbeck, M.: Decline in global oceanic oxygen content during
763 the past five decades, *Nature*, 542, 335–339, <https://doi.org/10.1038/nature21399>, 2017.

764 Smith, R., Jones, P., Briegleb, B., Bryan, F., Danabasoglu, G., Dennis, J., Dukowicz, J., Eden,
765 C., Fox-Kemper, B., Gent, P., Hecht, M., Jayne, S., Jochum, M., Large, W., Lindsay, K.,
766 Maltrud, M., Norton, N., Peacock, S., Vertenstein, M., and Yeager, S.: The Parallel Ocean
767 Program (POP) Reference Manual Ocean Component of the Community Climate System Model
768 (CCSM) and Community Earth System Model (CESM) 1, 2010.
769
770 Storch, D., Menzel, L., Frickenhaus, S., and Pörtner, H. O.: Climate sensitivity across marine
771 domains of life: Limits to evolutionary adaptation shape species interactions, *Glob Chang Biol*,
772 20, 3059–3067, <https://doi.org/10.1111/gcb.12645>, 2014.
773
774 Tiano, L., Garcia-Robledo, E., Dalsgaard, T., Devol, A. H., Ward, B. B., Ulloa, O., Canfield, D.
775 E., and Peter Revsbech, N.: Oxygen distribution and aerobic respiration in the north and south
776 eastern tropical Pacific oxygen minimum zones, *Deep Sea Res 1 Oceanogr Res Pap*, 94, 173–
777 183, <https://doi.org/10.1016/j.dsr.2014.10.001>, 2014.
778
779 Vaquer-Sunyer, R. and Duarte, C. M.: Thresholds of hypoxia for marine biodiversity, 2008.
780
781